http://dx.doi.org/10.17159/2411-9717/2017/v117n8a14

The benefits and knowledge gained in refractory testing with slag and nickel matte

by D. Gregurek*, V. Reiter*, A. Franzkowiak†, A. Spanring†, B. Drew†, C. Pichler‡, and D.R. Flynn§

Synopsis

Post-mortem studies of the lining refractories in the top-blown rotary converter (TBRC) at Stillwater Mining Company showed severe corrosion due to slag attack and high levels of sulphur. This led to a two-year collaborative project aimed at obtaining a better understanding of the wear phenomena and improving the refractory lining life in the TBRC. Initially, a complete phase chemical characterization was carried out. This was followed by FactSage™ calculations based on the slag and matte samples provided. The information from these sources fed into rotary kiln tests conducted at various process temperatures with several selected magnesia-chromite and alumina-chromia bricks in combination with a calcium ferritic slag. During the second year of the investigation a detailed test programme with nickel matte and preselected refractory brands was undertaken in the pilot TBRC at the University of Leoben, Austria. The detailed phase chemical investigation and the results and outcome of the tests are described in detail. A vital insight has been gained into the properties of a slag-matte system not previously studied. Additionally, the refractory wear trigger in the TBRC vessel has been identified, using time-lapse techniques, as the high-temperature spikes resulting from this highly exothermic desulphurization reaction. To limit refractory wear in service, the high-temperature spikes should be retarded by restricting the availability of fuel and the oxygen.

Keywords

refractories, magnesia-chromite bricks, post-mortem studies, calcium ferritic slag, nickel matte, rotary kiln, TBRC corrosion resistance test.

Introduction

In pyrometallurgy, owing to the challenges arising continuously from changing feed and the processing of more complex materials, metal producers are continuously adapting and optimizing their processes to new conditions (Davenport *et al.*, 2011; Crundwell *et al.*, 2011). In numerous cases the performance of pyrometallurgical processes is influenced by knowledge and control of the slag (Pawlek, 1983; Colclough, 1925; Sorokin *et al.*, 1994). The importance of good slag-making can be typically summed up by the old adage in smelting lore, 'look after your slag and the metal will look after itself' (Colclough, 1925). However, it is not only the plant operators who acknowledge the importance of the slag; it is also the furnace designers and refractory suppliers, who realize that knowledge of slag chemistry and the impact of the slag on the refractory are important for the optimization of refractory campaigns to improve equipment availability (Colclough, 1925; Sorokin *et al.*, 1994; Gregurek *et al.*, 2014). The detail in these ideas is discussed in this paper.

In the nonferrous metal industry, particularly in copper- and nickel-smelting furnaces, magnesia-chromite bricks are the refractory of choice because of their high corrosion resistance imparted by properties of the amphoteric species (Routschka and Wuthnow, 2012; Rigaud, 2011). Nevertheless, the refractory lining is exposed to complex wear caused by chemical, thermal, and mechanical stresses (Barthel, 1981; Gregurek and Majcenovic, 2003). Therefore an extensive understanding of the wear phenomena through post-mortem studies is an important requirement for the refractory producer, as it provides the basis for both customer recommendations and innovative product development.

RHI AG collaborates with many clients in order to achieve the optimum refractory solution for a given metal production process. The arrangement enables targeted refractory development, a better process understanding, and ultimately, lower operating costs. To achieve this goal the RHI Technology Center Leoben (TCL) in Austria combines practical corrosion-testing techniques and equipment such as an induction furnace, rotary kiln, cup tests, and drip-slag tests together with microscopic analyses followed by pilot-scale trials to arrive at a comprehensive understanding of brick wear (Gregurek *et al.*, 2013).

Throughout a two-year collaborative project between Stillwater Mining Company in the USA and RHI AG, practical tests were

* *RHI AG, Technology Center Leoben, Leoben, Austria.*

† *RHI AG, Vienna, Austria.*

‡ *CD Laboratory University of Leben, Leoben, Austria.*

§ *Stillwater Mining Company, Columbus, USA.*

 ISSN 2225-6253. Paper received Nov. 2015; revised paper received May. 2017.

carried out with different refractory types (selected magnesia-chromite and alumina-chromia bricks), utilizing 120 kg of calcium ferritic slag and 215 kg of nickel matte provided by Stillwater. The tests were conducted in a rotary kiln and in a pilot top-blown rotary converter (TBRC).

A detailed multi-stage programme was considered to be crucial to obtain a better understanding of refractory performance. The initial characterization of the slag and matte, with complete chemical and mineralogical analysis, was followed by a determination of melting points measured with a heating microscope and from thermochemical data in FactSage™. Finally, pilot-scale tests were carried out.

This paper provides an insight into the corrosion test work conducted at TCL and the value gained from post-mortem examinations.

Post-mortem investigation and analytical procedure

Generally, each post-mortem investigation starts with a visual inspection carried out on a section of the brick, followed by selection of samples for chemical analysis and phase chemical examination. The chemical analyses were carried out by X-ray fluorescence spectroscopy (XRF; Bruker S8 TIGER). The phase chemical investigation was conducted on polished sections with a reflected-light microscope and scanning electron microscopy (SEM; JEOL JSM-6460) combined with energy-dispersive and wavelength-dispersive X-ray spectrometry. Additionally slag and matte samples were investigated by X-ray diffractometry (XRD; Bruker D8 ADVANCE).

The post-mortem investigation was carried out on used refractory (magnesia-chromite brick of type 60:40) from the working lining of the TBRC at Stillwater Mining Company. The refractory life was 105 heats. The residual brick thickness was 170–180 mm. The immediate refractory hot face was slightly declined and covered with a thin coating of slag (Figure 1a). Cracks running parallel to the brick hot face could be observed.

Chemical analysis showed considerable enrichment of the refractory hot face with CaO, Fe_2O_3, NiO, and CuO (Table I). Some CoO and sulphur were also detected.

The mineralogical investigation revealed the following microstructural changes and areas (Figures 1b–1d):

- At the immediate hot face a 0–2 mm reaction layer consisting of Fe-Ni-Cr-(Mg-Co) oxide, Ni-Fe-Cu-Co-Mg oxide, and Ca-Fe oxide of the type dicalcium ferrite (C_2F) was observed (Deer, Howie, and Zussman, 1992)
- Behind this to a depth of approximately 15 mm from the hot face, the microstructure had degenerated completely and was brittle. The typical microstructure of the product containing coarse grains and fines was no longer visible, and the individual brick components could barely be distinguished. Owing to iron oxide enrichment of the magnesia component, an Mg-Fe oxide of magnesia-wüstite type had formed (Figure 1b). Chromite was heavily corroded by iron oxide (Figure 1c), a reaction resulting in the formation of Mg-Ni-Al-Cr-Fe oxide
- In the zone and area between 15–25 mm from the hot face the brick microstructure had been infiltrated by Ca-Al-Fe oxide. The oxide filled the pores. Owing to diffusion the chromite rims were enriched in iron oxide. These iron oxide-containing melts tend to equilibrate with chromite. Therefore the margins of chromite crystals already showed a higher iron content. Nevertheless, the chromite composition was not homogeneous with respect to iron content: the diffusivity of iron ions was not sufficient to achieve chemical equilibrium in the time available. Additionally, microscopic inspection showed that magnesia fines and calcium silicates acting as binder phases had been lost. Nevertheless, the reaction products were not present at the same location. Microscopic investigation of the cold end helps to explain this (see below)
- Below this, up to a depth of approximately 35 mm from the hot face, the brick microstructure was infiltrated with Cu-Fe sulphide and Ni-(Fe) sulphide
- At the refractory cold face the sulphur-based corrosion of the magnesia and the interstitial phase within the magnesia were visible. The main reaction products were Ca sulphate and Mg sulphate (Figure 1d). Obviously, sulphur attack caused the corrosion observed in the vicinity of the hot face. Melts containing Mg^{2+}, Ca^{2+}, and SO_4^{2-} percolated to the cold end, where the temperature remained above the respective invariant points. The separation of the reaction products from the reactants hindered chemical equilibrium close to the hot face. Therefore conditions for corrosion were maintained.

Figure 1e shows the virgin brick microstructure for comparison. The brick is based on fused magnesia-chromite and chromium ore.

Characterization of slag and matte

The first step prior to the experimental work was the characterization of the slag and matte samples from Stillwater Mining, which is described in the following sections.

Table I

Chemical analysis of the magnesia-chromite brick from the TBRC (wt%)

Sample	MgO	Al_2O_3	SiO_2	SO_3[1]	CaO	Cr_2O_3	Fe_2O_3[2]	NiO	CoO	CuO
Hot face (2–20 mm)	35	5	1	1	5	12	34	4	0.4	2
Unused brick	54.5	7.5	0.8		0.8	23.0	13.0			

[1]Total sulphur determined as SO_3
[2]Total iron determined as Fe_2O_3

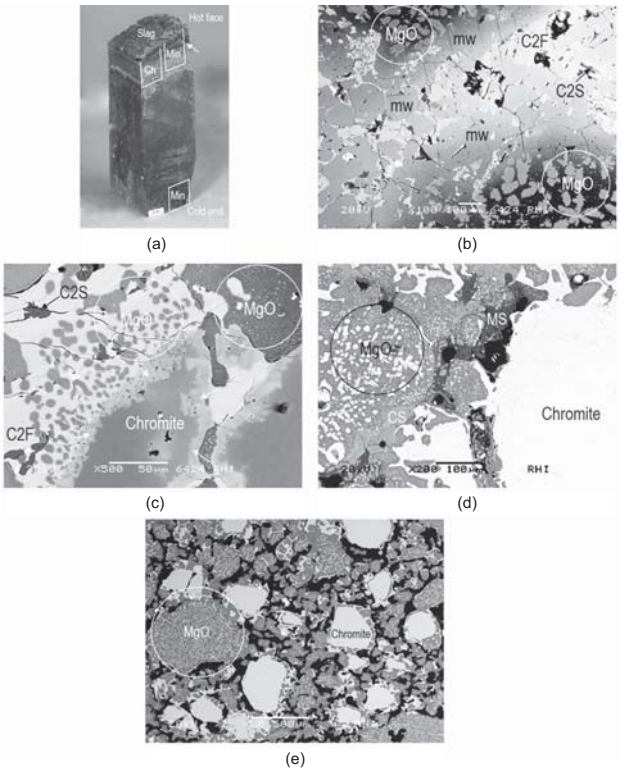

Figure 1—(a) Macroscopic view of used magnesia-chromite brick from the TBRC. Partly declined brick hot face covered with a thin coating of slag. A crack is parallel to the hot face (arrow). Samples for chemical analysis (Ch) and phase-chemical examination (Min) are indicated. (b) Microstructural detail approximately 5 mm from the hot face. Corroded magnesia-component (MgO) with the formation of magnesia-wüstite at rims (mw). Calcium ferrite (C_2F) enriched with Cr_2O_3. Dicalcium silicate (C_2S). (c) Microstructural detail approximately 10 mm from the hot face. Severe corrosion of chromite. At rims of chromite, formation of Ni-Ca-Mg-Fe-Al-Cr oxide (white arrows). (d) Microstructural detail of brick cold end. Sulphur attack of the magnesia component (MgO) and interstitial phase. Mg sulphate (MS) and Ca sulphate (CS) are the main reaction products. (e) Microstructural detail, with original brick microstructure for comparison. Magnesia component (Mg)

Slag characterization

The slag is a Ni-, Cu-, and S-rich Ca-Fe oxide (calcium ferritic-type slag – Table II). The main slag components include two different Ca-Fe oxides (one of type C_2F) and Ni-Mg-Fe-(Cr)-(Co) oxide of type magnesia-ferrite (Figures 2a and 2b).

Different Cu-(Fe)-Ni-(Pd) sulphide inclusions – predominantly Ni sulphide (Ni_3S_2, heazelwoodite), Cu sulphide (Cu_2S, chalcocite), and Pd-Pt-enriched Cu-Fe-Ni sulphide – were found in the slag. In addition to the phase chemical investigation, the melting point was determined with a heating microscope (Luidold, Schnideritsch, and Antrekowitsch, 2011). The melting temperature determined lay between 1350°C and 1410°C (measurements were carried out in air). Liquidus and solidus temperatures were estimated with the help of FactSage™ for the composition of slag and matte (Bale *et al.*, 2002). Under oxidizing conditions the calculated solidus and liquidus temperatures of slag were, respectively, 1057°C/1111°C and 1481°C/1424°C.

Matte characterization

The matte is a Ni-Cu-Fe-Co–bearing sulphide containing precious metals such as platinum and palladium (Table III). However, owing to a lack of standards and an overlap between palladium and rhodium spectra (rhodium-bearing XRF spectrometer), the exact palladium content could not be determined. Traces of Al_2O_3 and SiO_2 (<1 wt%) were also detected.

From phase chemical examination and X-ray diffractometry, we determined the main components of solid nickel matte to be Fe-Ni sulphide (pentlandite), Ni sulphide, and Cu-Fe sulphide (chalcopyrite) (Figures 2c and 2d). A Pt-

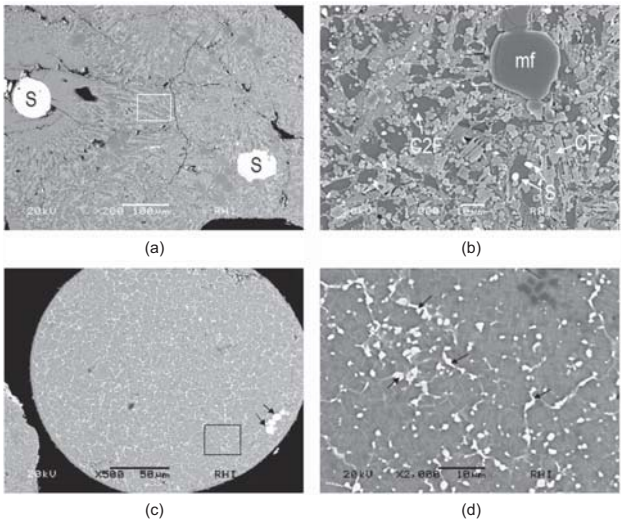

Figure 2—(a) Typical microstructural detail of granulated calcium ferritic slag with Cu-(Fe)-Ni-(Pd) sulphide inclusions (S). (b) Detail from Figure 2a. Ca-Fe oxides of type calcium ferrite (CF) and dicalcium ferrite (C2F). Ni-Mg-Fe-(Ca)-(Cr)-(Co) oxide of type magnesia-ferrite (mf). Sulphide inclusions (S). (c) Typical microstructural details of granulated matte. Pd, Pt-enriched Cu-Fe-Ni sulphide (arrows). (d) Detail from Figure 2c

Table II

Chemical analysis (by XRF) of the sample of slag from Stillwater Mining Company (wt%)

Na_2O	MgO	Al_2O_3	SiO_2	SO_3[1]	CaO	Cr_2O_3	Fe_2O_3[2]	NiO	CoO	CuO	PbO
0.3–0.8	1–2	0.5–0.6	1	5–9	15–19	0.7–0.9	48–58	8–15	0.5	4–7	0.1–0.3

[1]Total sulfur determined as SO_3
[2]Total iron determined as Fe_2O_3

Table III

Chemical analysis (by XRF) of the sample of matte from Stillwater Mining Company (wt%)

Pt	Pd*	S	Fe	Ni	Co	Cu	Zn	Pb	All_2Ol_3	CaO
0.3	–	21	30	34	0.6	13	0.1	0.3	0.6	0.6

*Could not be determined

and Pd-bearing Fe-Ni-Cu-Co-S phase was also detected. Some traces of calcium ferritc slag granules were also observed.

The phase constitution and the liquidus temperature of the matte were calculated with FactSage™ in the same way as for the slag. The FTmisc database was used for the calculations (the liquid sulphide solution was called FTmisc-MATTE). The stable solid phases were determined to be (Fe,Ni,Cu)S (pyrrhotite), $(Fe,Ni,Cu)_9S_8$ (pentlandite), (Co,Cu,Fe,Ni,Pb):Vacancy, and $(Fe,Ni_2,Cu_2)S$. These phases are solid solutions. The solidus and liquidus temperatures of the matte were calculated to be 667°C and 1132°C respectively.

Selected refractories and experimental work

Selection of refractories

Five magnesia-chromite brands (MCB1, MCB2, MCB3, MCB4, and newly developed MCB5), as well as one alumina-chromia brand (ACB1), were selected for both rotary kiln tests. The MCB1 (type MCr 50, ISO 10081-2) represents a standard direct-bonded magnesia-chromite brick consisting of fused magnesia and chrome ore. MCB2 is a high-quality, dense magnesia-chromite brick (type MCr 50, ISO 10081-2) based on magnesia-chromite co-clinker (OXICROM™ sinter) and chrome ore. MCB3 and MCB4 are also high-quality magnesia-chromite bricks (type MCr 60) based on fused magnesia-chromite and chrome ore. The newly developed MCB5 brick contains fused magnesia-chromite and has a higher Cr_2O_3 content (Type MCr 40) (Gregurek *et al.*, 2012). ACB1 is an alumina-chromia brick (type ACr 60/30, ISO 10081-4) based on chromia-corundum and chromium oxide.

Testing in the pilot TBRC was carried out with three magnesia-chromite brands (MCB4, MCB6, and MCB7). MCB6 and MCB7 (type MCr 50, ISO 10081-2) represent high-quality magnesia-chromite bricks consisting of fused magnesia-chromite and chrome ore. The MCB7 is a dense magnesia-chromite brick.

The chemical analyses of all the brick brands are listed in Table IV.

Rotary kiln tests

In the rotary kiln, with a diameter of 92 mm, up to six different brick brands were installed and tested simultaneously (Figure 3a). The furnace was heated with a propane-oxygen mixture. The first rotary kiln test with calcium ferritic slag was carried out between 1500°C and 1550°C. The second rotary kiln test was conducted at 1650°C. Temperatures higher than in the Stillwater process were chosen to simulate a process duration of several months. Both tests were carried out for 20 cycles. During testing, 1.5 kg of slag was charged to the kiln per cycle.

Pilot TBRC tests

Testing with nickel matte in the pilot TBRC, which was heated by a methane-oxygen burner, was carried out at a process temperature of approximately 1650°C (Figure 3b). This temperature was chosen because of the rotary kiln test results: it generated an identical post-mortem structure at this temperature. Oxygen was added to remove sulphur (Figure 3c). In total four trials were carried out under different sets of process parameters. The process parameters for all tests are summarized in Table V.

After reaching a process temperature of 1650°C, oxygen was introduced into the TBRC, which resulted in a significant increase in temperature (test 1). To mitigate this effect the energy was reduced by lowering the total gas flow rate to the burner. After a converting time of approximately two hours a liquid matte was tapped from the furnace.

A comparison of different refractory materials is generally based on differences in their corrosion behaviour under similar process conditions. For this purpose an additional test (test 2) was undertaken. It included the use of an off-gas analyser to provide information about desulphurization in the treated material during the oxidation step. The main variables are plotted in Figure 4. To provide oxygen for desulphurization the air ratio (λ) was varied. The value of λ defines an oxygen surplus ($\lambda > 1$) or an oxygen-deficient proportion ($\lambda < 1$) during the process.

At the starting point of the measurement ($t = 0$ minutes) all the material was charged into the furnace. After a few minutes, the first measurement with a type-S thermocouple was taken (1490°C). The temperature of the liquid bath was measured. Increasing λ resulted in a release of energy due to the reaction between sulphur and oxygen. A reduction in the

Table IV

Chemical analyses of several brands of RHI refractory used for testing (wt%)

Brand	MgO	Al_2O_3	SiO_2	CaO	Cr_2O_3	Fe_2O_3[1]	ZrO_2
MCB1	50.0	8.0	0.8	0.8	26.0	14.0	
MCB2	58.0	6.0	0.5	1.2	20.0	14.0	
MCB3	62.0	6.5	0.8	0.7	18.5	11.5	
MCB4	67.0	3.5	0.4	0.6	23.0	5.3	
MCB5	46.3	13.0	0.4	0.3	27.5	10.0	
MCB6	54.5	7.5	0.8	0.8	23.0	13.0	
MCB7	56.5	6.0	1.3	0.6	25.5	10.0	
ACB1		55.0	4.5		30.0	0.5	6.5

[1]Total iron determined as Fe_2O_3

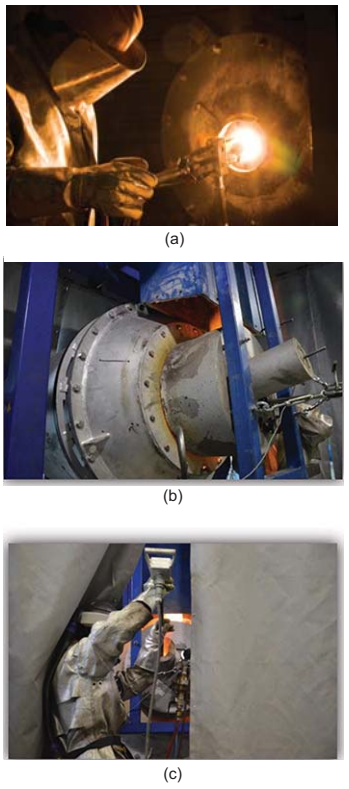

(a)

(b)

(c)

Figure 3—(a) Rotary kiln test at RHI Technology Center Leoben (TCL), during adjusting burner position after slag change. (b and c) Pilot TBRC testing at CD laboratory, University of Leoben, Austria. TBRC furnace during heating up (b) and during discontinuous temperature measurement for process control (c)

Table V

Process parameters for the pilot TBRC test

Test no.	1	2	3	4
Mass of charging matte [kg]	35	50	55	63
Temperature [°C]	1650	1650	1600	1600
λ	1–1.5	1–2	1–2.27	1.22

total gas flow rate (methane-oxygen) was used to mitigate this energy input through the exothermic oxidation of sulphur, by supplying small amounts of free oxygen.

The effect of increasing oxygen content (with constant oxygen flow though the burner) on temperature was determined after 60 minutes. This led to temperatures higher than the maximum of the thermocouple (for type-S limited to <1750°C, as shown in Figure 4). These two initial trials built the basis for the subsequent analysis of the pilot TBRC refractory lining. After trials 1 and 2, a new vessel was prepared for two additional trials with the same refractories.

The occurrence of exothermic reactions caused by the oxidizing treatment was evident in trials 3 and 4. Also evident was the stability of the refractory under process conditions. For a better comparison of different linings, the linings should be exposed to test conditions over several batches. These two trials, therefore, were consequently undertaken with the same brand of brick as used in the initial trial.

As mentioned, unlike tests 1 and 2, the subsequent trials 3 and 4 were carried out under constant temperature. In test 3, λ was varied under a constant gas flow rate, whereas in test 4 the burner capacity was varied under constant λ. With both variations the same result was achieved; nevertheless, the control of the furnace was much easier when maintaining the burner power at constant λ (Figure 5).

Results of the experimental work with slag

The macroscopic overviews of selected bricks after testing are shown in cross-section in Figure 6a–e. Two different measures are used to describe refractory performance in contact with slag, namely the area and depth for wear and infiltration respectively. The measure for wear describes the amount of refractory material that was removed during testing. The subsequent infiltration shows the area that was in contact with slag. The results from both trials, following determination of the wear area and wear depth across the final cross-sectional profile, are presented in Tables VI and VII. The main results of the phase chemical investigations are shown in Figures 7a–f.

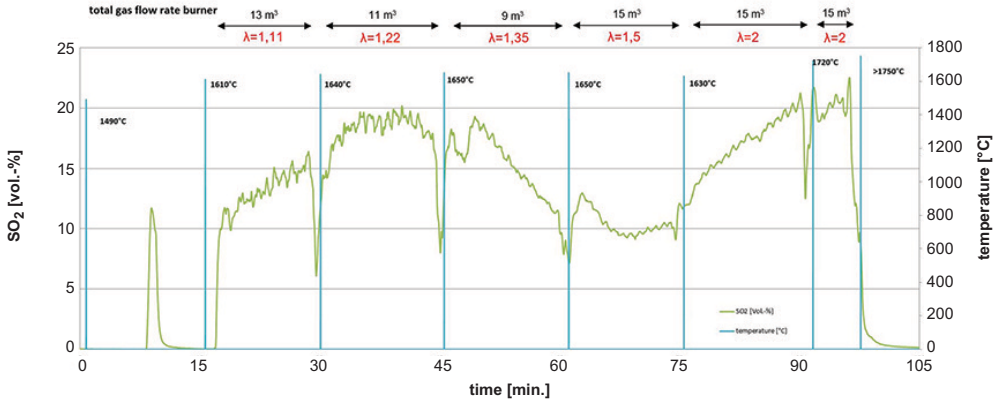

Figure 4—An example of temperature measurement during the first two TBRC tests. The temperature was continuously measured by a thermocouple in the TBRC gas room. For process control a discontinuous temperature measurement of the liquid matte was taken every 15 minutes, shown as spikes in the chart. Additionally, λ and the total gas flow rate were recorded

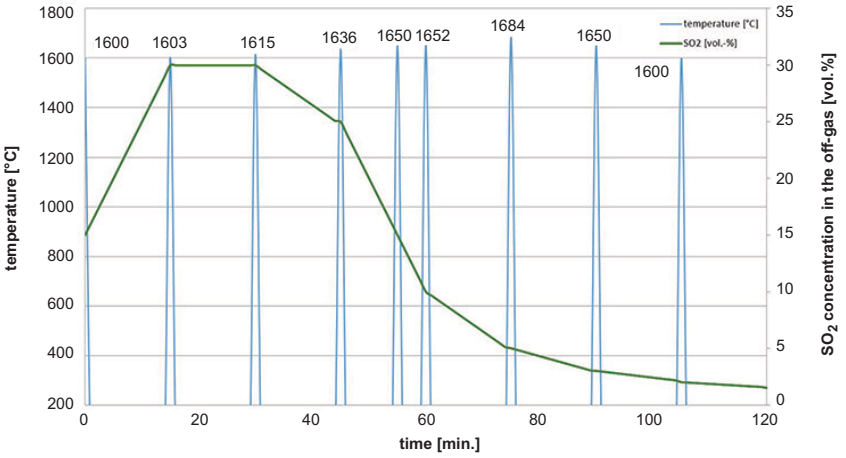

Figure 5—Example of the temperature and SO_2 content of the off-gas during tests 3 and 4. For process control the temperature of the liquid matte was measured (discontinuously) every 15 minutes, shown as spikes in the diagram

Table VI

Extent of wear and corrosion in the rotary kiln test (trial at 1500°–1550°C)

Brick brand	Wear area* (cm^2)	Wear depth* (mm)	Infiltration area* (cm^2)	Infiltration depth* (mm)
MCB1	2	4	54	28
MCB2	2	3	41	20
MCB3	0	0	43	21
MCB4	0	0	38	20
MCB5	0	0	46	24
ACB1	65(1)	5(1)	94	>20

*Based on macroscopic wear evaluation from the final cross-sectional profile
(1)Not representative due to high thermal shock

Table VII

Extent of wear and corrosion in the rotary kiln test (trial at 1650°C)

Brick brand	Wear area* (cm^2)	Wear depth* (mm)	Infiltration area* (cm^2)	Infiltration depth* (mm)
MCB1	25	22	104	50
MCB2	15	14	94	46
MCB3	20	18	94	47
MCB4	10	12	85	45
MCB5	24	21	105	56
MCB6	15	14	94	44

•Based on macroscopic wear evaluation from the final cross-sectional profile

Rotary kiln test at 1500–1550°C

All brick samples tested showed cracks caused by thermal shock during kiln operation. In the magnesia-chromite brick brands, either minimal or no wear was visible (Table VI). The greatest infiltration depth was identified in MCB1. The high wear observed for the alumina-chromia brick ACB1 can be explained by crack formation caused by thermal shock from the initial testing and subsequent loss of refractory

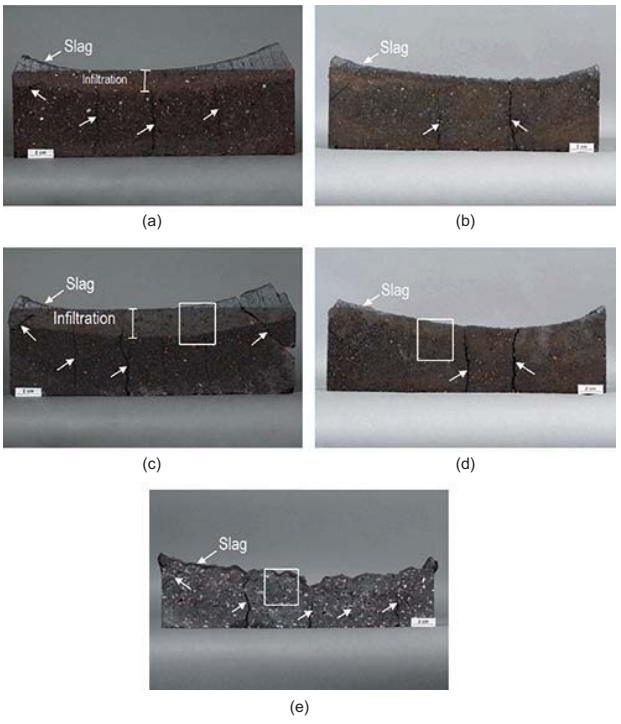

Figure 6—Cross-sectional view of selected magnesia-chromite MCB4 (a, b), MCB1 (c, d), and alumina-chromia ACB1 (e) bricks after the rotary kiln test at 1500–1550°C (left side: a, c, e) and 1650°C (right side: b, d). A slag coating covers the immediate brick hot face. Crack formations are indicated with white arrows. Polished sections were prepared from the portions indicated by white rectangles

The main microstructural changes to the magnesia-chromite bricks investigated, after the rotary kiln test, are summarized below (for example MCB1, see Figures 7a and 7b).

The immediate brick hot face was covered with a 1–2 mm thick reaction zone. Within this area the magnesia component was completely dissolved. Only some chromite relics were still visible. Below the reaction zone a deep-reaching infiltration by calcium ferrite and corrosion of the brick microstructure was observed.

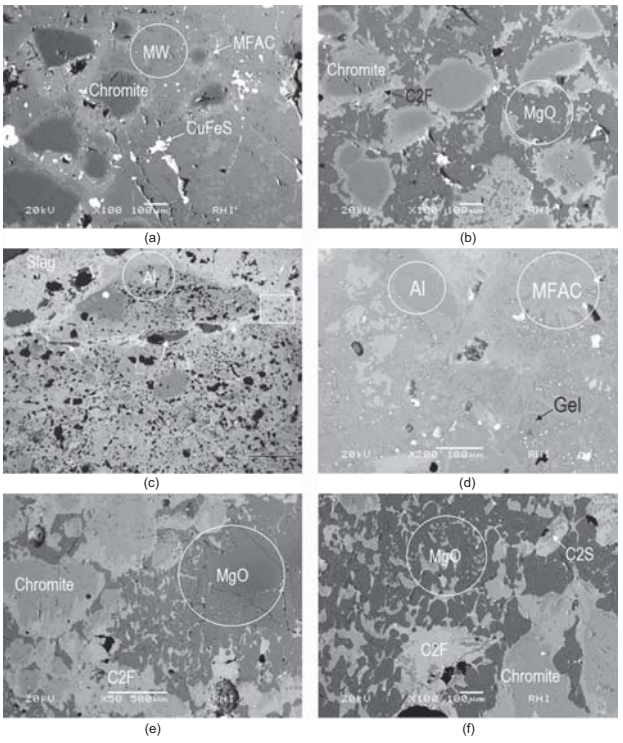

Figure 7a–b—Microstructural details in the magnesia-chromite brick MCB1 after the rotary kiln test at 1500–1550°C, approximately 2 mm (a) and 10 mm (b) from hot face. Severe corrosion and degeneration of the brick microstructure. Corroded magnesia (MgO) and chromite. Formation of Ni–rich magnesia-wüstite, (Ni)-Fe-Mg oxide (MW), Mg-Fe-Al-Cr oxide of spinel structure (MFAC), calcium ferrite (C_2F) enriched with Cr_2O_3, and CuFeS from matte infiltration. Figure 7c–d Microstructural details of the alumina-chromia brick ACB1 after the rotary kiln test at 1500–1550°C. (c) Immediate brick hot face. Below the slag coating, infiltrated and corroded brick microstructure was observed. The crack that formed parallel to the hot face is partly filled with slag (arrows). Corroded fused alumina (Al). (d) Detail from Figure 7c, showing degenerated, recrystallized, and infiltrated brick microstructure. Mg-Fe-Al-Cr oxide of spinel structure (MFAC). The Ca-Al silicate is gehlenite, $Ca_2Al_2SiO_7$ (Gel). Figure 7e–f Microstructural details of the magnesia-chromite brick MCB1 after rotary kiln test at 1650°C. Corrosion of the magnesia and chromite was significantly higher than in the first rotary kiln test at 1500–1550°C. Corroded MgO and chromite. Calcium ferrite (C_2F) enriched with Cr_2O_3. Dicalcium silicate (C_2S)

In the infiltrated and completely degenerated brick microstructure (0–5 mm from the hot face) the single brick components could no longer be distinguished. The high supply of Fe oxide resulted in the formation of a low-melting Ni-rich magnesia-wüstite ([Ni]-Fe-Mg oxide). The chromite and chromite precipitates (Routschka and Wuthnow, 2012) were corroded. Owing to the corrosion of chromite, (Ca)-Mg-Fe-Al-Cr oxide and (Ca)-Fe-Cr-Al oxide of spinel structure formed. In Figure 7a the brick is partly infiltrated by matte.

In the case of the alumina-chromia brick ACB1 (Figures 7c–d), infiltration of the microstructure can be traced over the entire polished section (0–20 mm from the hot face). Nevertheless, the greatest microstructural changes were observed in the area 0–2 mm from the hot face. In that area of the brick, pore-filling infiltration, recrystallization of a Cr-corundum–bearing matrix, corrosion of a Zr mullite, and the formation of Mg-Fe-Al-Cr oxide and (Na)-Ca-Al silicate of type gehlenite ($Ca_2Al_2SiO_7$) took place. The immediate hot face was covered with a 1–2 mm thick reaction zone. In the infiltrated brick microstructure, cracks formed parallel to, but also vertical to, the hot face. These cracks were partly filled with slag.

Rotary kiln test at 1650°C

Owing to the high wear observed during the test, the alumina-chromia brick ACB1 was replaced by magnesia-chromite brick MCB6. Compared with the first rotary kiln test, the refractory wear and the infiltration depth for all bricks were significantly higher (Table VII). In cross-section, the greatest wear was observed for MCB1/MCB5 and the lowest for MCB2.

Phase chemical investigation revealed the brick microstructure in MCB1 to be highly degenerated, especially between 0–20 mm from the hot face. Infiltration, corrosion of both brick components (magnesia and chromite), and the formation of a low-melting Cu-Ni-rich magnesia-wüstite were observed after the second rotary kiln test (Figures 7e and 7f). Nevertheless, the microstructural changes were much more distinctive than those in the first rotary kiln test at 1500–1550°C. The chromite rims were highly enriched in Fe oxide and Ni oxide (Figure 8). Additionally, owing to the decomposition and oxidation of Cu-Fe-Ni sulphide, sulphur attack and formation of sulphur-bearing phases could be observed at the end of infiltration.

Thermodynamic calculations

The interactions of different combinations of refractory materials with the calcium ferritic slag can be described thermodynamically in respect of the potential reaction products formed at the interface and the solubility of the refractory components in the slag.

The calculations were run in FactSage™ for temperatures of 1550°C and 1650°C under oxidizing conditions. The phase constitution of a system was calculated under the assumption that the defined elements or compounds of the system react entirely or partially to reach a state of chemical equilibrium. Reaction kinetics were not considered in the thermochemical calculations.

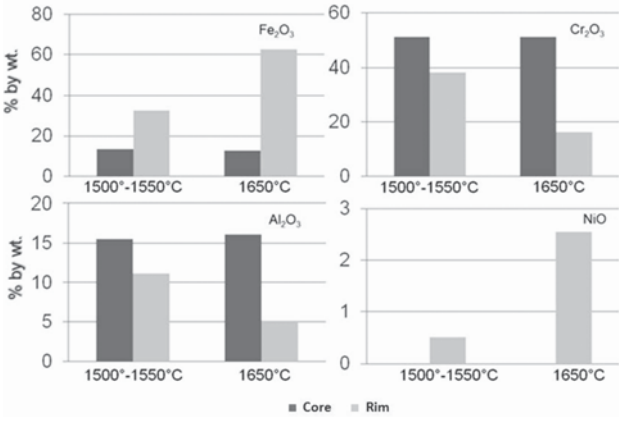

Figure 8—Magnesia-chromite brick MCB1. Significant differences in the chemical composition of chromite at the rim and core at two different test temperatures

The equilibrium phases and phase compositions were determined on the basis of the refractory-slag ratio. For this purpose a variable <*A*> was introduced, which is defined as the mass ratio of refractory material to the total mass of refractory plus slag. <*A*> = 0 describes the composition of a slag not in contact with refractory, and <*A*> = 100 describes the composition of a refractory that is not in contact with slag.

The slag amount as a function of <*A*> was compared for the different refractory bricks (see Figures 9a and 9b) at 1550°C and 1650°C. The alumina-chromia brick showed a considerably higher solubility than the magnesia-chromite brands. The refractories can be ranked according to solubility, which increases in the order:

MCB4 < MCB5 < MCB3 < MCB1 < MCB2

Of the magnesia-chromite bricks investigated, the MCB4 brick shows the lowest solubility. However, the difference in solubility between the various brands, with the exception of MCB2, is small.

Results of the experimental work with matte

During the first two tests in the pilot TBRC none of the tested magnesia-chromite brick brands showed wear. In cross-section, the deeply infiltrated brick microstructure over the whole cross-section (approx. 60 mm from the hot face) was visible (Table VIII). Only in the case of brick MCB6 was the infiltration depth 47 mm from the hot face (Figure 10a).

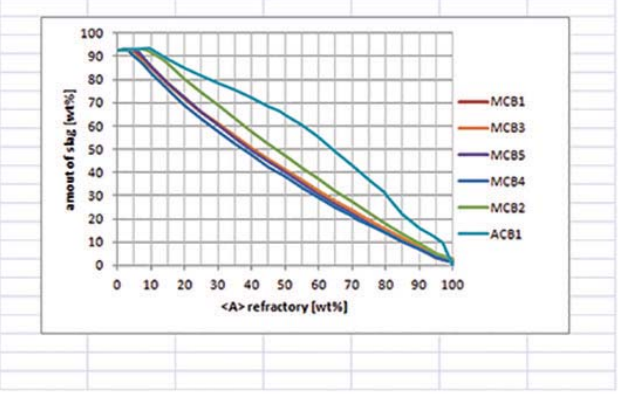

(a)

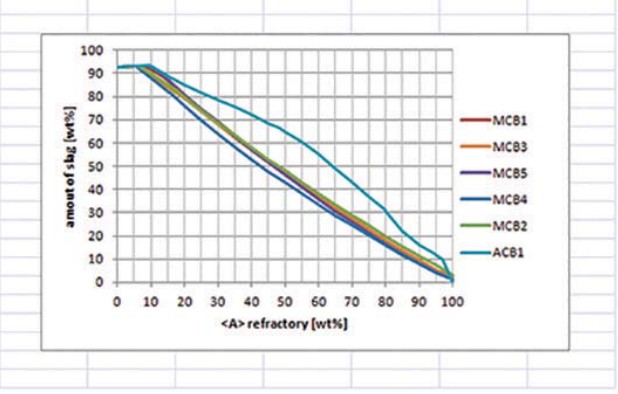

(b)

Figure 9—FactSage™ calculations of slag amounts at 1550°C (a) and 1650°C (b)

Table VIII

Results of the first two TBRC tests at 1650°C

Brick brand	Wear area* (cm^2)	Wear depth* (mm)	Infiltration area* (cm^2)	Infiltration depth* (mm)
MCB4	–	–	142–196	60
MCB6	–	–	128–172	47
MCB7	–	–	153–201	60

*Based on macroscopic wear evaluation from the final cross-sectional profile

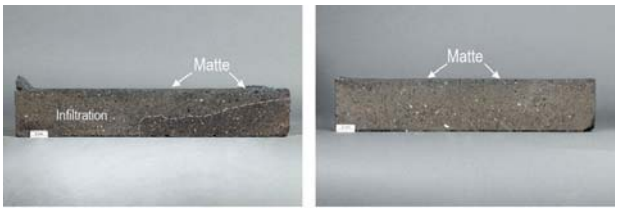

(a) (a)

Figure 10—Cross-sectional view of selected magnesia-chromite brick MCB6 after TBRC trials 1 and 2 (a), and 3 and 4 (b). Matte coating covering the immediate brick hot face

After tests 3 and 4, all tested magnesia-chromite bricks showed almost no wear, although a deep-reaching infiltration of the brick microstructure over the complete cross-section (Figure 10b) was observed.

Owing to similar wear behaviour in all trials, the main microstructural changes can be summarized as follows.

- All samples showed a thin reaction zone (0–2 mm from the hot face). Within this zone a strongly degenerated and recrystallized brick microstructure was visible. The coarse grains and the matrix fines in the brick could no longer be distinguished. The magnesia component was highly enriched in Fe oxide and Ni oxide. The chromite precipitates and the rims of chromite grains were also enriched in these oxides
- Below the reaction zone a deeply infiltrated brick microstructure could be observed. The main infiltrate was a (Cu)-Fe-Ni–bearing sulphide (Figure 11a)
- During the first two tests, the corrosion of magnesia by sulphur was minimal
- During the final two tests (3 and 4), the corrosion of magnesia fines and the coarse magnesia grains by sulphur was significant. Idiomorphic and newly precipitated MgO crystals and Ca sulphate were also observed (Figure 11b).

Summary and conclusions

The post-mortem studies carried out on refractories in the TBRC at Stillwater Mining Company showed the following features.

- Aggressive chemical attack due to calcium ferritic slag. The attack manifests as a deep-reaching infiltration of the brick microstructure and corrosion of brick components, virgin magnesia, and chromite

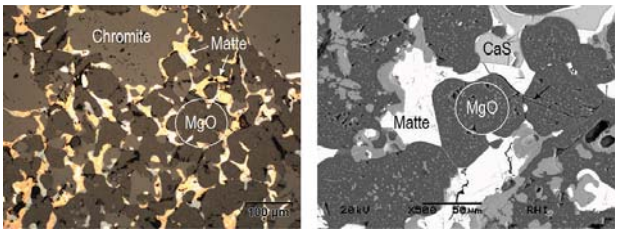

(a) (b)

Figure 11—Typical microstructural details of MCB6 after trials 3 and 4. Reflected-light microscopy (a) and scanning electron microscopy (b). Approximately 10 mm from the hot face. Infiltrated and corroded brick microstructure, showing corroded magnesia component (MgO), mickel matte,.and idiomorphic Ca sulphate (CS)

- Such a degenerated brick and brittle microstructure is highly susceptible to crack formation and spalling, especially in the case of frequent thermal shocks typical of TBRC operation.

These phenomena lead to decreased refractory performance and lifetime.

The chemical characterization of slag and matte, particularly the determination of the melting points, was important for experimental work.

The following observations can be summarized from the from both rotary kiln tests.

- There was significantly higher wear and infiltration of the brick microstructure at 1650°C for the same number of cycles. The lowest wear and infiltration, especially at 1650°C, was displayed by the MCB4 brick
- There was sulphur attack and the formation of sulphur-bearing phases at the limit of infiltration owing to the decomposition and oxidation of Cu-Fe-Ni sulphide
- As in the post-mortem study, there was severe degeneration of the brick microstructure due to chemical attack by the calcium ferritic slag. The microstructural changes were more distinctive than those in the first rotary kiln test at 1500–1550°C, which led to the chosen TBRC temperature
- Compared with the magnesia-chromite bricks, the alumina-chromia brick ACB1 showed significantly higher wear due to thermal shock
- FactSage™ showed that magnesia-chromite bricks withstand the calcium ferritic slag better than the alumina-chromia brick in respect of the solubility of refractory in the slag.

The main results of four pilot TBRC tests carried out with nickel matte can be summarized as follows.

- Unlike the refractory in the rotary kiln tests, there was no macroscopically visible wear due to hot erosion. Nevertheless, during tests 3 and 4 complete infiltration of the brick microstructure by matte occurred
- All tested magnesia-chromite bricks showed similar and deep-reaching infiltration of the brick microstructure over the whole cross-section (0–60 mm from the hot face). During the first two trials, only the MCB6 brick showed slightly lower infiltration depths
- In the first 2 mm beneath the hot face, the brick microstructure was strongly recrystallized. This resulted from the massive supply of Fe-Ni oxide caused by the oxidation of the nickel matte. This microstructural degeneration is similar to that seen in the rotary kiln test
- During the first two tests, the expected sulphur attack from the oxidation of nickel matte did not occur
- During tests 3 and 4, a significantly more aggressive sulphur attack in the infiltrated brick microstructure was observed
- The most important issue during the pilot TBRC test work was the exceptionally rapid rise in temperature due to the exothermic reaction caused by SO_2 formation.

To replicate accurately the refractory wear mechanisms in the multi-stage production process, a dual test programme utilizing both a rotary kiln and a TBRC was required. The evaluation of the simulated process samples in the multi-stage production showed identical features on the macro and micro scales to those seen in the initial post-mortem evaluation, thereby validating the original findings.

A vital insight has been gained into the properties of a slag-matte system not previously studied. Additionally, the refractory wear trigger has been identified in the TBRC vessel, using time-lapse techniques, as the high-temperature spikes resulting from this highly exothermic desulphurization reaction. To limit refractory wear in service, the high-temperature spikes should be retarded by restricting the availability of fuel and oxygen required to maintain this highly exothermic reaction.

The recommendations from this work have been implemented by the client, and the advantages are already apparent. The development of compatible refractory materials for this matte-slag system enabled client-oriented and tailor-made refractory solutions to be implemented that promoted smooth and efficient operations with increased campaign life.

References

Bale, C.W., Bélisle, E., Chartrand, P., Decterov, S.A., Eriksson, G., Hack, K., Jung, I.-H., Kang Y.-B., Melançon, J., Pelton, A.D., Robelin, C., and Petersen, S. 2002. FactSage thermochemical software and databases – recent developments. *Calphad*, vol. 33, no. 2. pp. 295–311.

Barthel, H. 1981. Wear of chrome magnesite bricks in copper smelting furnaces. *Interceram*, vol. 30. pp. 250–255.

Colclough, T.P. 1925. A study of the reactions of the basic open-hearth furnace. *Transactions of the Faraday Society*, vol. 21. pp. 202–223.

Crundwell, F.K., Moats, M.S., Ramachandran, V., Robinson, T.G., and Davenport, W.G. 2011. Extractive Metallurgy of Nickel, Cobalt and Platinum-Group Metals. Elsevier, Oxford. pp. 147–158.

Davenport, W.G., King, M., Schlesinger, M., and Biswas, A.K. 2011. Extractive Metallurgy of Copper. Elsevier, Oxford.

Deer, W.A., Howie, R.A., and Zussman, J. 1992. An Introduction to the Rock-Forming Minerals. 2nd edn. Pearson Education, Essex. 3–15 pp.

Gregurek, D. and Majcenovic, C. 2003. Wear mechanism of basic brick linings in the nonferrous metals industry – Case studies from copper smelting furnaces, *RHI Bulletin*, vol. 1. pp. 17–21.

Gregurek, D., Ressler, A., Reiter, V., Franzkowiak, A., Spanring, A., and Prietl, T. 2013. Refractory wear mechanisms in the nonferrous metal industry: Testing and modeling results. *Journal of Metals*, vol. 65, no. 11. pp. 1622–1630.

Gregurek, D., Spanring, A., Ressler, A., and Breyner S. 2012. High performance brands for the nonferrous metals industry. *Proceedings of the International Smelting Symposium*, Orlando, Florida, 11–15 March, The Minerals, Metals & Materials Society, Warrendale, PA. pp. 39–46.

Gregurek, D., Wenzl, C., Reiter, V., Studnicka, H.L., and Spanring, A. 2014. Slag characterization: A necessary tool for modelling and simulating refractory corrosion on a pilot scale. *Journal of Metals*, vol. 66, no. 9. pp. 1677–1686.

Luidold, S., Schnideritsch, H., and Antrekowitsch, H. 2011. Schmelzmetallurgische Beurteilung von nichteisen-metallhältigen Schlacken (Melt metallurgical assessment of non ferrous slag). *Berg- und Huettenmännische Monatshefte*, vol. 156, no. 1. pp. 1–5.

Pawlek, F. 1983. Metallhüttenkunde. Walter de Gruyter, Berlin.

Rigaud, M. 2011. Corrosion of refractories and ceramics. *Uhlig`s Corrosion Handbook*. 3rd edn. Revie, R.W. (ed.). Wiley, Hoboken, NJ. pp. 387–398.

Routschka, G. and Wuthnow, H. 2012. Handbook of Refractory Materials. 4th edn. Vulkan-Verlag, Essen.

Sorokin, M.L., Bystrov, V.P., Nikolaev, A.G., and Komkov, A.A. 1994. Thermodynamic of nickel matte converting. *Proceedings of a Symposium sponsored by the Extraction and Processing Divison Pyrometallurgical Committee*, San Francisco, California, 27 February–3 March. The Minerals, Metals & Materials Society, Warrendale, PA. pp. 59–69.